Direction Finding Antenna Systems

Author

NOMAN AHMAD

Regn Number

MSEE-2K21 : 00000362849

Supervisor

Dr. NOSHERWAN SHOAIB

DEPARTMENT OF ELECTRIAL ENGINEERING

SCHOOL OF ELECTRICAL ENGINEERING & COMPUTER SCIENCE (SEECS)

NATIONAL UNIVERSITY OF SCIENCES AND TECHNOLOGY

ISLAMABAD

November, 2023

Direction Finding Antenna Systems

Author

NOMAN AHMAD

Regn Number

MSEE-2K21 : 00000362849

A thesis submitted in partial fulfillment of the requirements for the degree of

Master of Science (Electrical Engineering)

Thesis Supervisor:

Dr. NOSHERWAN SHOAIB

DEPARTMENT OF ELECTRICAL ENGIEERING (RF & MW)

SCHOOL OF ELECTRICAL ENGINEERING & COMPUTER SCIENCE

NATIONAL UNIVERSITY OF SCIENCES AND TECHNOLOGY
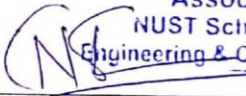
ISLAMABAD

November, 2023

THESIS ACCEPTANCE CERTIFICATE

Certified that final copy of MS/MPhil thesis entitled "Direction Finding Antenna Systems" written by Noman Ahmad, (Registration No 362849), of SEECS has been vetted by the undersigned, found complete in all respects as per NUST Statutes/Regulations, is free of plagiarism, errors and mistakes and is accepted as partial fulfillment for award of MS/M Phil degree. It is further certified that necessary amendments as pointed out by GEC members of the scholar have also been incorporated in the said thesis.

Signature: _____

Name of Advisor: _____Dr Nosherwan Shoaib_____

Date: _____11-Aug-2023_____

Associate Professor
NUST School of Electrical
Engineering & Computer Science

HoD/Associate Dean: _____

Date: ____30/11/2023____

Signature (Dean/Principal): _____

Date: _____

i

Approval

It is certified that the contents and form of the thesis entitled "Direction Finding Antenna Systems" submitted by Noman Ahmad have been found satisfactory for the requirement of the degree

Advisor :   Dr Nosherwan Shoaib

Signature: _____

Date: _____11-Aug-2023_____

Committee Member 1:Dr. Sajjad Hussain

Signature: _____

13-Aug-2023

Committee Member 2:Ahsan Azhar

Signature: _____

Date: _____11-Aug-2023_____

Signature: _____

Date: _____

ii

Dedicated to my exceptional parents and adored siblings whose tremendous support and cooperation led me to this wonderful accomplishment

Certificate of Originality

I hereby declare that this submission titled "Direction Finding Antenna Systems" is my own work. To the best of my knowledge it contains no materials previously published or written by another person, nor material which to a substantial extent has been accepted for the award of any degree or diploma at NUST SEECS or at any other educational institute, except where due acknowledgement has been made in the thesis. Any contribution made to the research by others, with whom I have worked at NUST SEECS or elsewhere, is explicitly acknowledged in the thesis. I also declare that the intellectual content of this thesis is the product of my own work, except for the assistance from others in the project's design and conception or in style, presentation and linguistics, which has been acknowledged. I also verified the originality of contents through plagiarism software.

Student Name:Noman Ahmad

Student Signature: _____

Acknowledgement

I am thankful to my Creator Allah Subhana-Watala to have guided me throughout this work at every step and for every new thought which You setup in my mind to improve it. Indeed, I could have done nothing without Your priceless help and guidance. Whosoever helped me throughout the course of my thesis, whether my parents or any other individual was Your will, so indeed none be worthy of praise but You.

I am profusely thankful to my beloved parents who raised me when I was not capable of walking and continued to support me throughout in every department of my life.

I would also like to express special thanks to my supervisor Dr. Nosherwan Shoaib for his help throughout my thesis and also for Advanced RF Measurements and Microwave Devices and Systems courses which he has taught me. I can safely say that I haven't learned any other engineering subject in such depth than the ones which he has taught.

I would also like to pay special thanks to Dr. Haq Nawaz for his tremendous support and cooperation. Each time I got stuck in something, he came up with the solution. Without his help I wouldn't have been able to complete my thesis. I appreciate his patience and guidance throughout the whole thesis.

I would also like to thank Dr. Sajjad Hussain and Dr. Ahsan Azhar for being on my thesis guidance, evaluation committee and for their support and cooperation.

Finally, I would like to express my gratitude to all the individuals who have rendered valuable assistance to my study.

Table of Contents

List of Abbreviation

Abbreviation	Definition
ADC	Analog-to-Digital-Convertor
AoA	Angle-of-Arrival
APS	Angular-Pseudo-Spectrum
DF	Direction-Finding
DoA	Direction-of-Arrival
FoV	Field-of-View
RF	Radio-Frequency
RMSE	Root-Mean-Square-Error
SNR	Signal-to-Noise-Ratio
SPDT	Single-Pole-Double-Throw
SP4T	Single-Pole-Quadruple-Throw

List of Tables

List of Figures

Abstract

Monopulse antenna systems have attracted a lot of attention in radar, military and other wireless communication applications where determining the direction-of-arrival (DoA) is required. Monopulse antenna systems are employed to determine direction-of-arrival (DoA) where the angle of arrival (AoA) is measured using a single pulse. One of the most significant advantages of this type of system is its speed of operation. As all of the necessary computations are performed in the hardware that are available instantly. In amplitude monopulse technique, absence of phase information results in angular ambiguities that causes false angle-of-arrival (AoA) estimation in given field-of-view (FoV). Such angular ambiguity in sign ($\pm$) associated with AoA has been addressed with phase-based power summation property of 90° hybrid coupler and orthogonal switched-beams.

Key Words: *Beam-Switching, Corporate-Feeding, Direction-of-Arrival, Linear Polarization, Mono-Pulse, Orthogonal Switched Beams, Sequential-Lobing.*

1. Introduction

In this work, the use of orthogonal switched-beams at $\theta = \pm20^o$ is proposed to improve the robustness against angle-of-arrival (AoA) ambiguities in amplitude comparison monopulse systems compared to the conventional use of only sum (Σ) and difference (Δ) patterns. As monotonic behavior of monopulse function inside the given field-of-view causes angular ambiguity so such false detection can be mitigated while analyzing the echo signal through additional switched beams. Theoretical and experimental results using a corporate-fed 1×2 patch array antenna integrated with 3 dB / 180° and 3 dB / 90° hybrid couplers, which synthesizes a sum, difference patterns and two orthogonal switched beams ($\theta = \pm20^o$) at 3 GHz, endorse this improvement. The proposed antenna system can also find applications in sequential lobing based direction finding systems.

2. Literature Review

Monopulse antenna systems have attracted a lot of attention in radar, military and other wireless communication applications where determining the direction-of-arrival (DoA) [1-2] is required. They are well known due to their high speed, high accuracy, and target estimation through a single pulse. In amplitude comparison monopulse technique, due to absence of phase information, the echo signal inside the field-of-view (FoV) region can create angular ambiguities, which causes false angle-of-arrival (AoA) estimation. A new mechanism to mitigate such angular ambiguities in conventional monopulse antenna systems is reported in [3]. In [3], the RF-multiplier was used to determine the sign associated with the AoA. At higher frequencies, the cost of such phase comparators is increased. Likewise, high speed analog to digital convertors (ADC) and RF-Down-Sampling Circuit are required to convert the higher frequency i.e., RF signals to digital signals for signal processing i.e., phase comparison (in this case) leads to additional cost in system.

In [4-6], mechanically rotated antennas have also been employed to determine the AoA without angular ambiguity. In this method, the associated monopulse function (Δ/Σ) is obtained through the signals received from the two antennas. Although, the angular ambiguity has been resolved using mechanically rotated two antennas, however this non-planar geometry can only be used in passive direction finding (DF) antenna system due to absence of sum (Σ) pattern.

Moreover, this method also reduces the resultant FoV of monopulse function. As, these switched beams have been synthesized mechanically, the same can be realized with planar antenna by employing the 3 dB / 90° hybrid coupler as presented in this work. The literature review is also summarized in Table 1-1.

Table 1-1: Summary of Literature Review

References.	Centre Frequency	Bandwidth	Field-of-View	Angular Ambiguity Resolution Schemes	Remarks
[3]	9.85 GHz	149 MHz	76°	RF-Multiplier	o At higher frequencies, the cost of such phase comparator is increased. o Planar Antenna. o Active and Passive DF.
[4]	866.5 MHz	3.0 MHz	50°	Mechanically Rotated Antennas	o Non-planar Antenna. o It can only be used in passive DF systems.
[5]	2.45 GHz	Not Given.	50°		
[6]	2.45 GHz	20 MHz	60°		

In this chapter, a new mechanism is proposed for the improvement of amplitude comparison robustness against false detection while deploying a simple planar-antenna system. The proposed system resolves the angular ambiguities without utilizing the phase information or phase comparator. It is based upon the use of two additional orthogonal switched beams ($\theta = \pm 20^o$) along with sum and difference patterns. The orthogonality in antenna beams reduces the interferences in the directions where other switched beams have their relative maxima. Thus, the two orthogonal switched beams have been employed to mitigate such interferences. Section 1.2 discusses the theoretical back ground of the presented DF antenna system to address the angular ambiguities which may occur in conventional monopulse antennas. The prototype of the proposed antenna system and the experimental results are described in section 1.3.
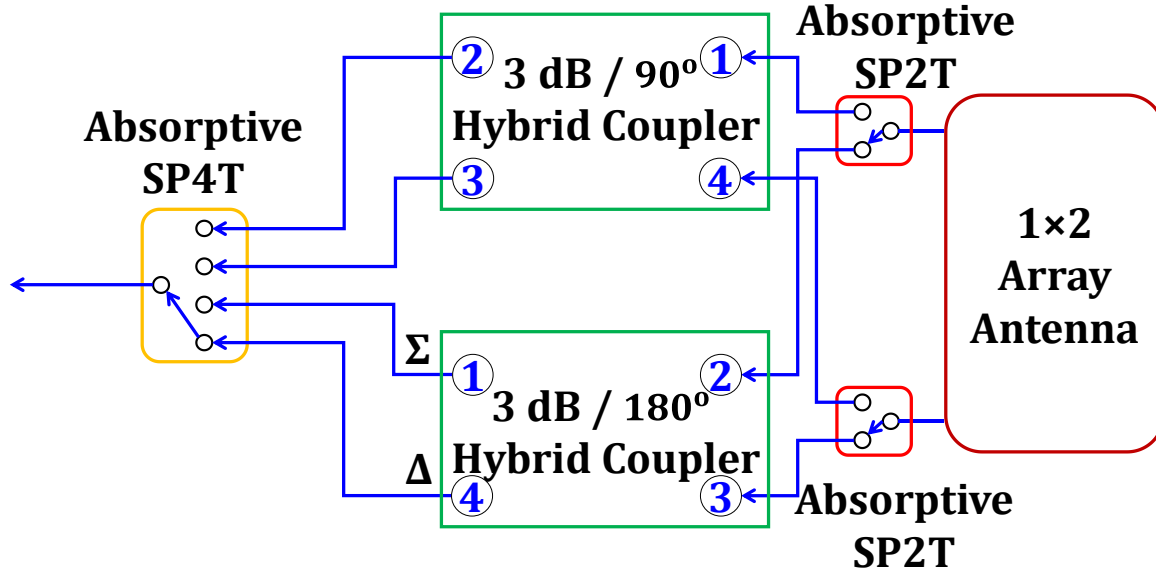
Figure 1.1: Block diagram of the proposed DF antenna system.

3. Methodology

The block diagram of the proposed DF antenna concept is shown in Figure. 1.1. The SP2T switches are utilized to interconnect the intended hybrid couplers with the antenna ports independently. The SP4T switch is incorporated in the circuit to interconnect the output ports of the hybrid couplers with a single envelope detector for a cost effective solution. The hybrid couplers are used as feeding network to synthesize the time-shared Σ, Δ patterns and orthogonal switched beams. In conventional monopulse systems, for instance at $\theta = \pm 20^\mathbf{o}$, the echo signals captured through Σ and Δ channels create equal amplitudes i.e., $\Sigma_1 = \Sigma_2$ and $\Delta_1 = \Delta_2$ which causes the ambiguity in AoA estimation as shown in Figure. 2.2(a). To resolve such ambiguity, two switched beams are introduced to distinguish the sign (+or-) associated with AoA as indicated in Figure. 2.2(b). In that case, a unique amplitude is captured from these switched beams to determine the accurate AoA.
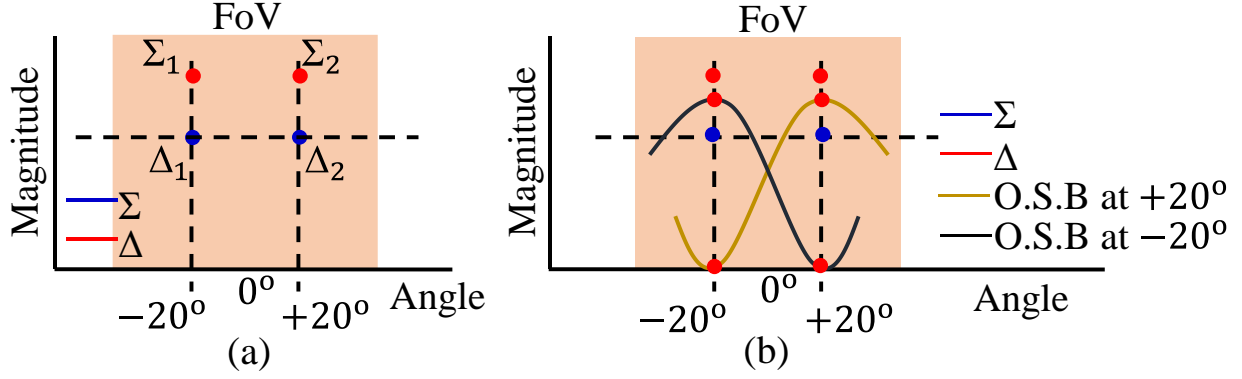
Figure 1.1: (a). Conventional sum (Σ) and difference (Δ) patterns for monopulse synthesis; (b). Proposed orthogonal switched beams with Σ and Δ patterns.

3.1 Amplitude-Comparison Monopulse DF

Based on the array factor theory, two isotropic point sources, spatially displaced by 0.75λ apart when excited with equal amplitude and phase difference of 0° / 180°, the Σ and Δ patterns are synthesized respectively [7-8].

$$f(\theta) = \Sigma = \cos\left(\frac{\beta d}{2} \times \sin\theta\right) \tag{1}$$

$$f(\theta) = \Delta = \sin\left(\beta\frac{d}{2} \times \sin\theta\right) \tag{2}$$

Taking ratio of equations (2) and (1) provides:

$$\frac{\Delta}{\Sigma} = \frac{\sin\left(\beta\frac{d}{2} \times \sin\theta\right)}{\cos\left(\beta\frac{d}{2} \times \sin\theta\right)} = \tan\left(\beta\frac{d}{2} \times \sin\theta\right) \tag{3a}$$

$$\theta = sin^{-1}\left(\frac{\lambda}{\pi d} \times tan^{-1}\left(\frac{\Delta}{\Sigma}\right)\right) \text{where } \beta = \frac{2\pi}{\lambda} \tag{3b}$$
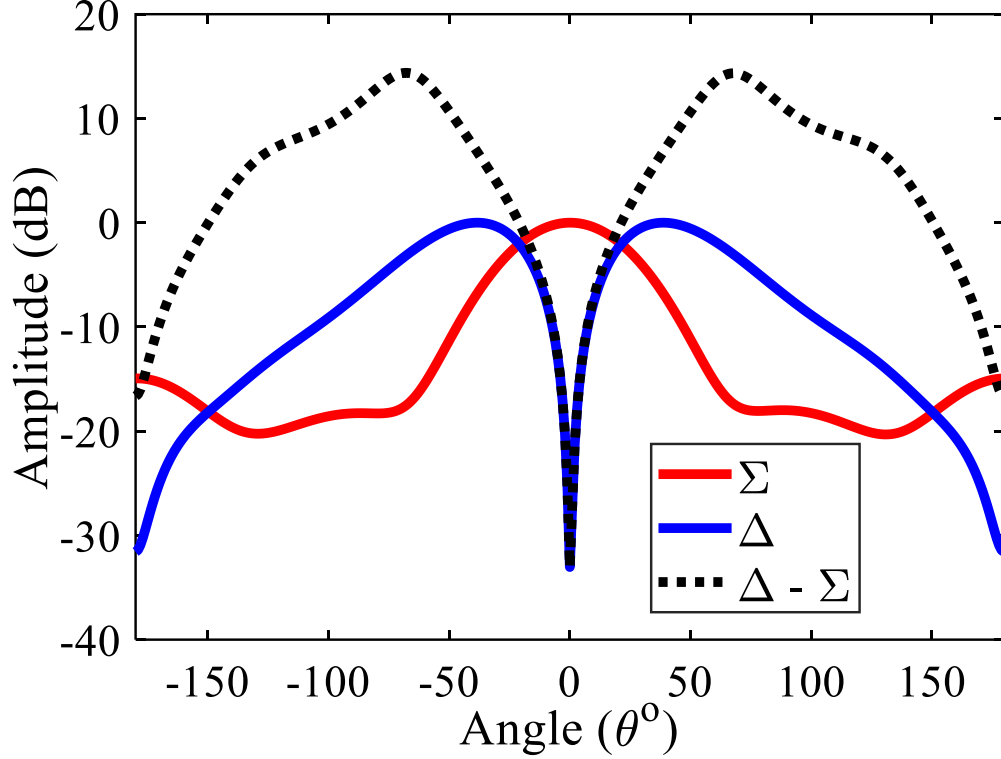
Figure 1.2: Simulated normalized sum (Σ) and difference (Δ) radiation patterns and the equivalent characterized monopulse function (Δ/Σ). Simulated Angular Pseudo Spectrum (APS) for the incident signal at θ = 20°

The equation (3) indicates that the AoA can be estimated by taking the ratio of Σ and Δ signals. The simulated Σ and Δ patterns and the calculated characterized mono-pulse function (Δ/Σ) are plotted in Figure. 1.3. In Δ-pattern, the null depth is observed to be less than -33 dB. The obtained FoV of 60° covers the sector spanning over +30° to -30°. The mono-pulse function is monotonic as it does not have unique value for a given AoA (θ) in the obtained FoV. For instance, for a given FoV, the mono-pulse function gives value of 0.1113 (linear) for θ = ±20°. So, a signal approaching from elevation angle (θ) of 20° can be interpreted as a signal coming from θ = -20° thus leading to false AoA estimation. This ambiguity emerges only when only the amplitude of the received signals is considered for the DF estimation. In Figure. 1.4, this is also illustrated through angular pseudo spectrum (APS) obtained when the mono-pulse value of the received signals is compared with the characterized monopulse function [4].

$$\text{APS}(\theta) = -20log_{10}\left(\frac{\Delta}{\Sigma}(\theta) - \frac{\Delta}{\Sigma}_{measured}\right) \tag{4}$$
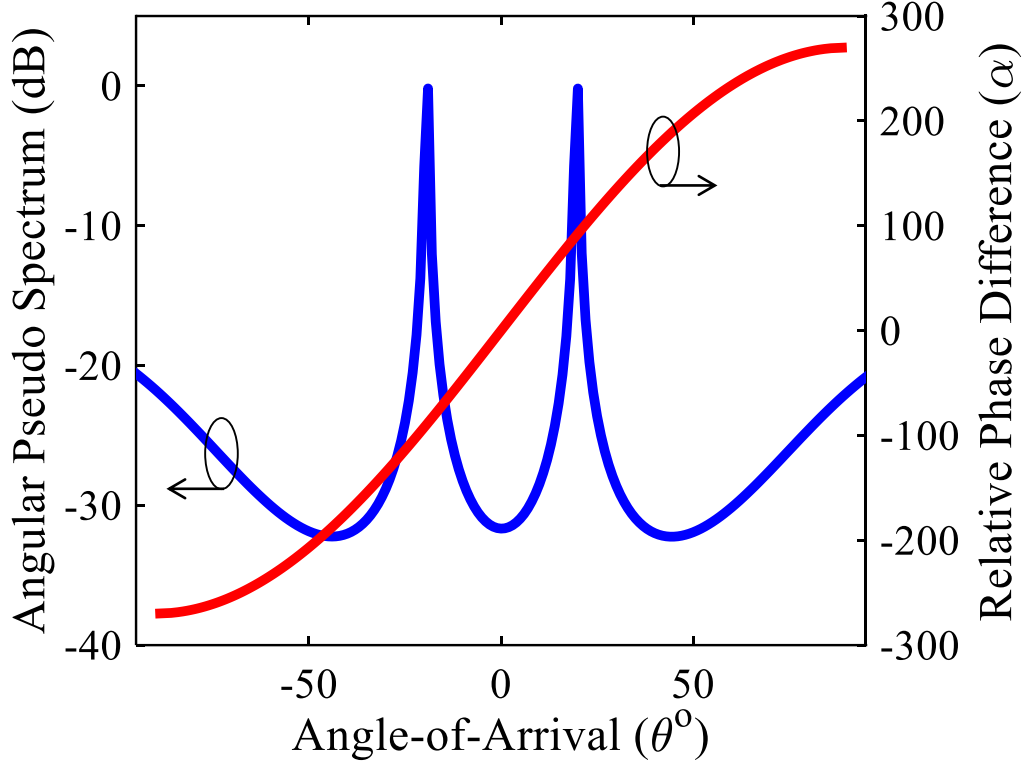
Figure 1.3: Simulated Angular Pseudo Spectrum (APS) for the incident signal at θ = 20º

In Figure. 1.4, the simulated APS is plotted for an incident signal at θ = 20⁰. In that case, the magnitude of the power received through the Σ and Δ channels lead to a mono-pulse function value of 0.1113 (linear), it creates a peak in the APS at the actual AoA = 20⁰. However, there is also another peak at θ = -20⁰ in the same FoV. This ambiguity is caused by the monotonic behavior of the mono-pulse function. Consequently, due to lack of phase information in amplitude-comparison monopulse systems, the sign associated with the AoA cannot be determined. Based on antenna array theory, if a signal coming from elevation angle (θ) impinges upon the array elements with inter-element spacing of 'd', it experiences a relative phase difference (α) among the elements [9].

$$\alpha = \beta \times d \times \sin(\theta) = sin^{-1}\left(\frac{\alpha}{\beta \times d}\right) \qquad (5)$$

$$\theta = sin^{-1}\left(\frac{\alpha}{\frac{2\pi}{\lambda} \times \frac{3\lambda}{4}}\right) = sin^{-1}\left(\frac{\alpha}{\frac{3\pi}{2}}\right) \qquad (6)$$

6

The graphical representation of equation (6) is given in Figure. 1.7 (a), that shows the relationship between the AoA and the corresponding 'α' among the array elements. For AoA > $0°$, the 'α' < $-0°$ likewise the α' > $-0°$ for AoA < $-0°$. To compute the relative phase difference between the incident signals, phase-based power summation property of the 3 dB / $90°$ hybrid coupler is exploited. . The S-parameters of the 3 dB / $90°$ hybrid coupler are given as:

$$\begin{bmatrix} O_1 \\ O_2 \\ O_3 \\ O_4 \end{bmatrix} = \left(\frac{-1}{\sqrt{2}}\right) \times \begin{bmatrix} 0 & j & 1 & 0 \\ j & 0 & 0 & 1 \\ 1 & 0 & 0 & j \\ 0 & 1 & j & 0 \end{bmatrix} \begin{bmatrix} I_1 \\ I_2 \\ I_3 \\ I_4 \end{bmatrix} \tag{7a}$$

The phasor form representation of associated outputs in terms of input currents for 3 dB / $90°$ hybrid coupler can be expressed as follows:

$$O_1 = \left(\frac{-1}{\sqrt{2}}\right) \times (jI_2 + I_3) \tag{7b}$$

$$O_2 = \left(\frac{-1}{\sqrt{2}}\right) \times (jI_1 + I_4) \tag{7c}$$

$$O_3 = \left(\frac{-1}{\sqrt{2}}\right) \times (I_1 + jI_4) \tag{7d}$$

$$O_4 = \left(\frac{-1}{\sqrt{2}}\right) \times (I_2 + jI_3) \tag{7e}$$

It is evident from (7b) to (7e) that the amplitudes of the outputs' signals vary based upon the phase of the input signals. For instance, assuming $I_1 \angle 0°, I_4 \angle 90°$ and $I_2 = I_3 = 0$, then $O_1 = O_4 = 0$ and the resulting outputs O_2, O_3 would be,

$$O_2 = \left(\frac{-jI_1 + I_2}{\sqrt[2]{2}}\right) = \left(\frac{-jI_1 + I_2 \angle 90°)}{\sqrt[2]{2}}\right) = \frac{I_1}{\sqrt[2]{2}}(-j + (cos(90°) + j\,sin(90°)) = 0 \tag{8}$$

$$O_3 = \left(\frac{I_1 - jI_2}{\sqrt[2]{2}}\right) = \left(\frac{I_1 - jI_2 \angle 90°)}{\sqrt[2]{2}}\right) = \frac{I_1}{\sqrt[2]{2}}(1 - j(cos(90°) + j\,sin(90°)) = \frac{2 \times I_1}{\sqrt{2}} \tag{9}$$

The basic vector notation of input signal and the resultant output signal for 3 dB / $90°$ hybrid coupler is also mentioned in Figure. 1.6. When signal 'I_1' at port-1 lags the signal 'I_4' at port-4 by a phase of $90°$, both I_1 and I_4 add constructively at port-2 and destructively at port-3, as shown in Figure. 1.5 (a). Likewise, I_1 and I_4 add destructively at port-2 but constructively at

port-3, when signal 'I_1' at port-1 leads the signal 'I_4' at port-4 by a phase of 90º, as mentioned in Figure. 1.5 (b). For any other phase difference at port-1 and port-4, the output would be the vector sum of the that input signals.
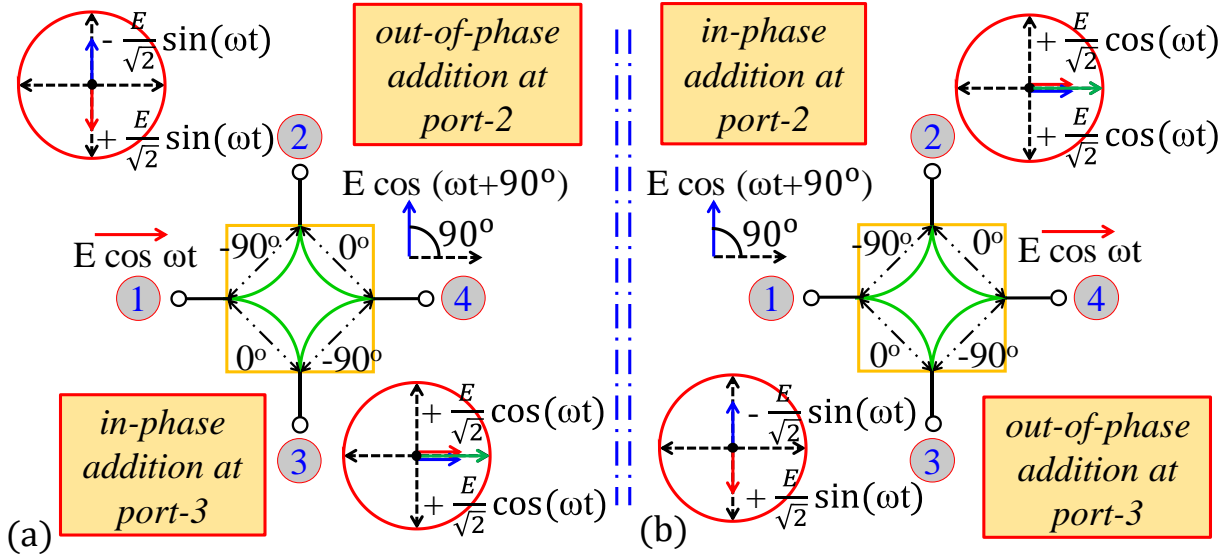
Figure 1.4: Basic vector notation of the input and output signals for 3 dB / 90º hybrid coupler, (a) port-1 lags port-4 by a phase of 90º and (b) port-1 leads port-4 by a phase of 90º.

Next, to analyze the phase-based power summation property 90º hybrid coupler, the relative phase difference between the input signals has been varied from $-180º$ to $180º$ and the resultant magnitude of the output signal has been observed as shown in Figure. 1.6.
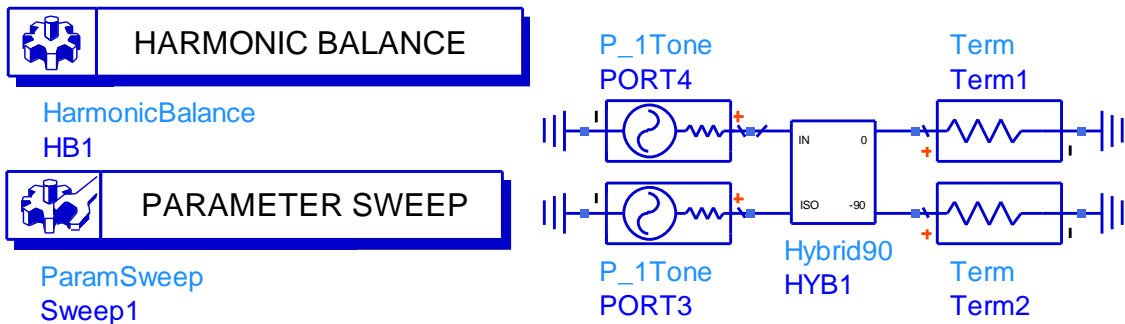
Figure 1.5: Schematic diagram of 3 dB / 90º hybrid coupler to compute the resultant magnitude of output signals, when relative phase difference between the input signals is varied from -180º to +180º.

The simulated magnitude of the output signals i.e., V_2 and V_3 of 3 dB / 90° hybrid coupler versus phase variation between applied signals i.e., V_1 and V_4 is plotted in Figure. 1.7 (b). It is evident that $V_2 > V_3$ for $0°<\alpha<90°$ (or $0°<\theta<20°$) and $V_2 < V_3$ for $-90°<\alpha<0°$ (or $-20°<\theta<0°$). The maxima of V_2 and V_3 exist at $\alpha = 90°$ ($\theta = 20°$) and $\alpha = -90°$ ($\theta = -20°$) respectively. Likewise, the minima of V_2 and V_3 exist at $\alpha = -90°$ ($\theta = -20°$) and $\alpha = 90°$ ($\theta = 20°$) respectively. On other hand, two isotropic point sources spatially displaced $\frac{3\lambda}{4}$ apart when excited with identical amplitude and $\pm 90°$ out of phase, the main beam switched at $\pm 20°$ in elevation plane. Mathematically,

$$\text{AF} = 1 \times e^{-j\beta\left(\frac{d}{2}\right)\cos\theta} + 1 \times e^{-j\left(\frac{\pi}{2}\right)}e^{j\beta\left(\frac{d}{2}\right)\cos\theta} \tag{10}$$

$$\text{AF} = e^{-j\left(\frac{\pi}{4}\right)}\left[e^{-j\left[\beta\left(\frac{d}{2}\right)\cos\theta - \frac{\pi}{4}\right]} + e^{j\left[\beta\left(\frac{d}{2}\right)\cos\theta - \frac{\pi}{4}\right]}\right] \tag{11}$$

$$\text{AF} = e^{-j\left(\frac{\pi}{4}\right)} \times \cos\left(\frac{\beta d}{2} \times \cos\theta - \frac{\pi}{4}\right) \tag{12}$$

Substituting the inter-element spacing (d) $= \frac{3\lambda}{4}$ and normalizing the equation it gives (6), which is maximum for $\theta = \pm 19.65°$.

$$f(\theta) = \cos\left\{\frac{3\pi}{4} \times \left(\sin\theta \pm \frac{1}{3}\right)\right\} \tag{13}$$

Thus the interconnection of 90° hybrid coupler with 1×2 array antenna generates two orthogonal switched beams at the elevation angle (θ) of 20° and $-20°$ in the *xoz*-plane. It can also be observed that the maximum gain and the null of both orthogonal switched beams are equivalent to voltage response of the 90° hybrid coupler in terms of its maxima and minima. Consequently, the sign (+ or -) associated with AoA can be measured through relative amplitudes of the 90° coupler.
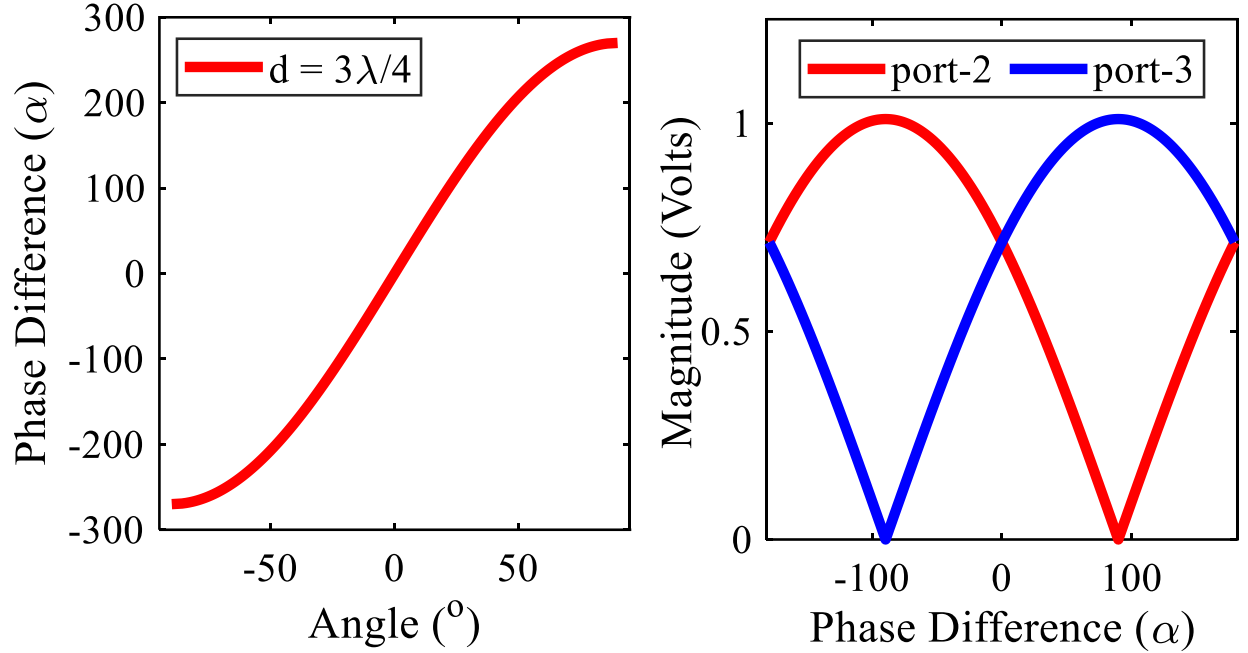
Figure 1.6: Left Side: Simulated relative phase difference (α) with respect to the angle of arrival (θ) for inter-element spacing equal to 0.75λ ; Right-Side: Simulated amplitude of the output voltage signals at port-2 and port-3 of the quadrature coupler versus relative phase variations (α) between input ports.

The timing diagram showing the compatibility of transmitted pulse with four switched beams in reception mode is shown in Figure 1.8. A pulse with duty cycle for instance 30% is transmitted through sum-pattern and corresponding echo signal is captured in listening time through four switched beams as shown in Figure. 1.8. On rising edge of echo signal i.e., $(T=\tau_0+\tau_1)+\tau_3$ sec; the antenna system will capture the echo signal for time 'τ_2' sec through the sum-pattern. Next, at '$T+\tau_2+2\tau_3$' sec; the antenna system will switch to Δ-pattern and it will receive the echo signal again for time 'τ_2' sec. Similarly, it will receive the echo signal through $\pm20^o$ switched beams at '$T+2\tau_2+3\tau_3$' sec and '$T+3\tau_2+4\tau_3$' sec respectively for the time 'τ_2' sec. The 'τ_3' incorporates the rise and fall time of SP2T and SP4T switches. With reference to Figure 1.8, the signal captured through pulse-1 and pulse-2 will be used for the estimation of AoA, whereas the magnitude of pulse-3 and pulse-4 would be compared to determine the sign ($\pm$) associated with AoA.
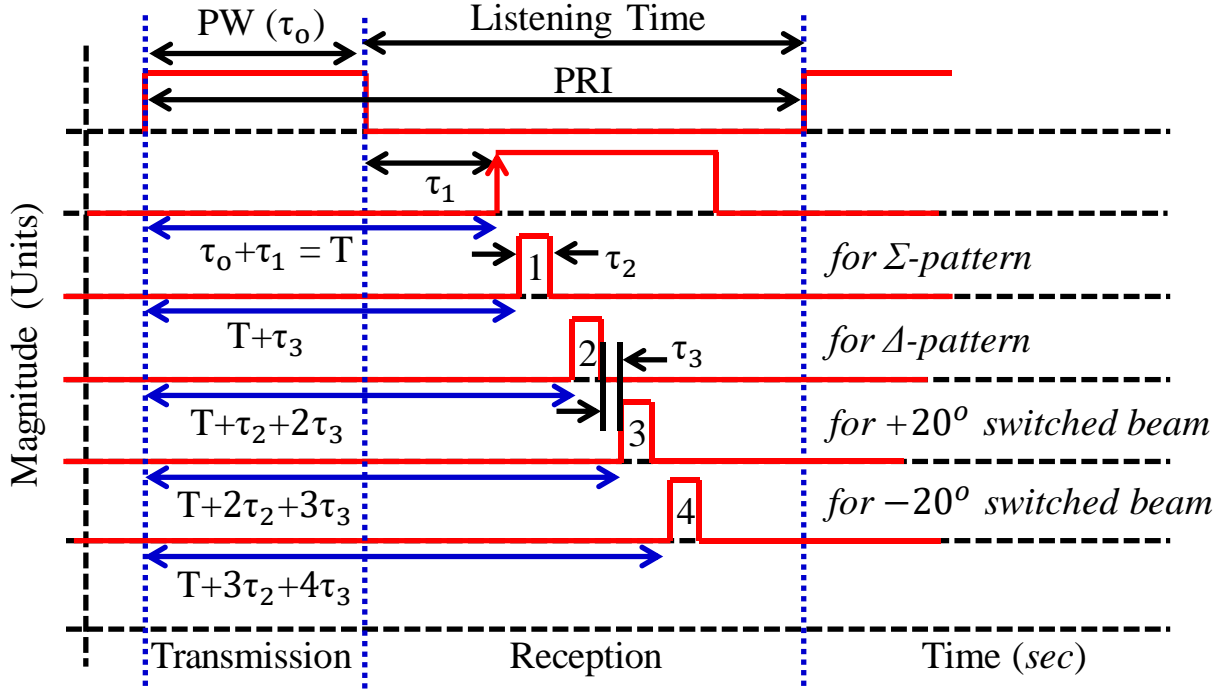
Figure 1.7: Timing diagram showing the compatibility of transmitted pulse with the four switched beams in reception mode; τ_1: round trip time ; PRI : pulse-repetition interval ; τ_2: time slot assigned to receive the echo signal through respective switched beams (20% of the pulse width (τ_o)) ; τ_3: it incorporates the rise and fall time of SP2T and SP4T switches (5% of the pulse width (τ_o)).

3.2 Amplitude-Comparison Sequential-Lobing DF

In sequential lobing, time-shared multiple switched beams are synthesized to locate the object's position by comparing the amplitude of the echo signal through each switched beam. The "DF Slope (m)" is the one of the important figure-of-merit, for instance, DF slope of $0.8 \frac{dB}{deg}$ means that every 1° of angle deviation induces an amplitude variation of 0.8 dB, however, it also reveal that that the amplitude measurement error of 1 dB causes the error $(1\ dB)/(0.8 \frac{dB}{deg}) = 1.25^o$ in measured AoA. Next, in practical scenario, the direction finding accuracy is defined over a fixed SNR. The DF accuracy will be degraded when noise level increases.
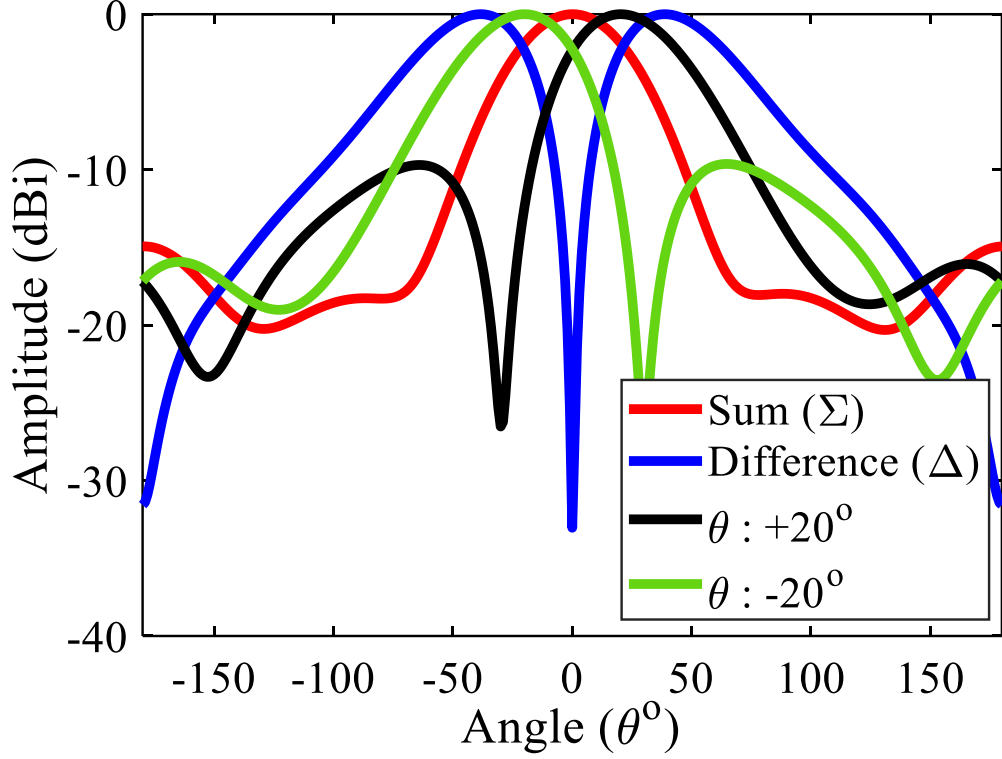
Figure 1.8: Simulated time-shared multiple beams for the sequential lobing based direction-finding systems.

The four switched beams will be comprised of sum, difference and two switched patterns at elevation angle (θ) of 20⁰, and -20⁰ respectively for 'α' set to 0⁰, 180⁰, 90⁰ and −90⁰. The required value of 'α' and associated switched beams are realized through the 90⁰ and 180⁰ hybrid couplers as summarized in Table 1-1.

Table 1-1: Realized Switched Beams based on equation. 6.

Beam No.	Inter-Element Spacing	Progressive Phase Difference (α)	Elevation Angle (θ)	Azimuth Angle (φ)
1.		0⁰	Sum Pattern	
2.	$\dfrac{3\lambda_o}{4}$	+90⁰	+20⁰	φ = 0⁰ (xoz-plane)
3.		−90⁰	−20⁰	
4.		180⁰	Difference Pattern	

The simulated radiation patterns of the time-shared switched beams are plotted in Figure. 1.9. The simulated DF slopes for different ranges of the AoA are also plotted in Figure. 1.10. Using the radiation patterns, the DF slopes are calculated by subdividing the entire FoV into sub-ranges based upon the intersection of two consecutive radiation patterns in magnitude ≥ -3 dB. For given subrange, the pattern with greater magnitude is subtracted from pattern with lesser magnitude to obtain the DF slopes for that subrange of AoA. The minimum DF slope is reported to be 0.2 dB/deg for 0° to +15° sector. The simulated DF slopes are linear, so the AoA can be determined without any ambiguity.
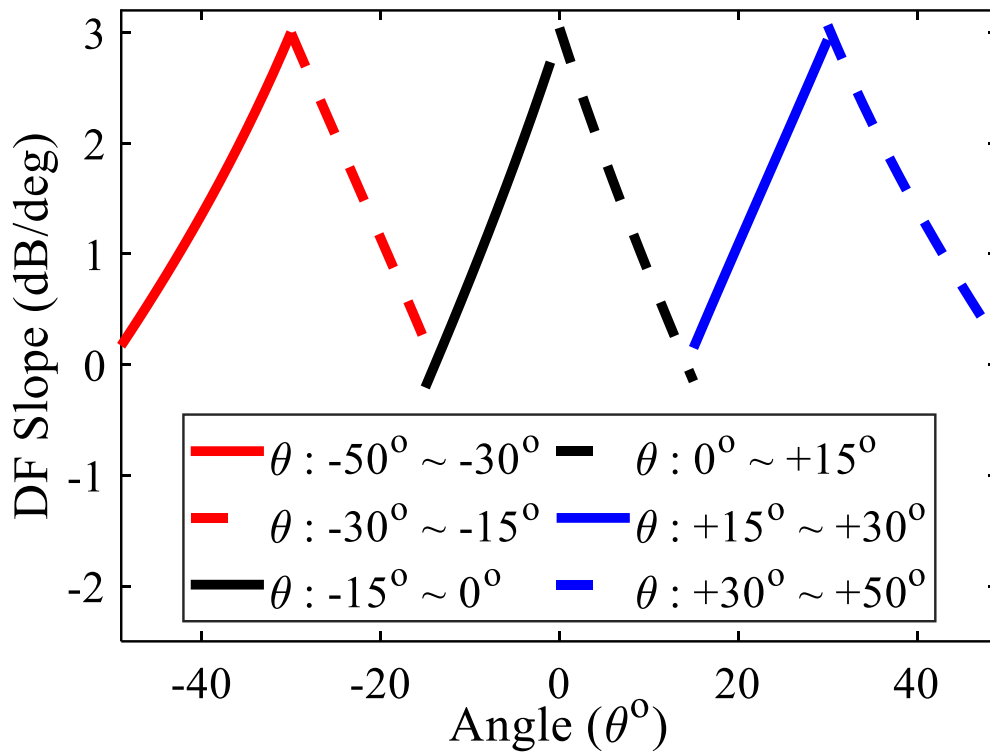

Figure 1.9: Simulated DF slopes (dB/deg) versus the angle-of-arrivals (AoA).

4. Results and Discussion

To validate the proposed DF antenna system, the two-port vertically polarized, 1×2 edge-fed square shaped patch array antenna, along with the 180° ring hybrid coupler and the 3 dB /90° hybrid coupler are fabricated using low-cost FR-4 substrate (ε_r= 4.4, tanδ = 0.02 and thickness =1.6 mm). The 90° and 180° hybrid couplers are connected to the input ports of the

1×2 array antenna using amplitude and phase matched RF coaxial cables as shown in Figure. 1.27 [9].

The prototype of the fabricated 1×2 array antenna is shown in Figure. 1.11. The radiating structure includes two edge-fed square shape patch ($l_p = l_p = 23mm$) elements with inter-element spacing 'd' of $\frac{3\lambda}{4}$. Based on antenna array theory, the inter-element spacing should not greater than λ_o in order to avoid the grating lobes. On other side, the mutual coupling among the array elements (which affects the active return loss) is inversely proportional to inter-element spacing. So, this is the optimum value to realize the maximum gain at the boresight i.e., $\theta = 0^o$, $\forall \varphi$ with minimal side lobes level (SLL).
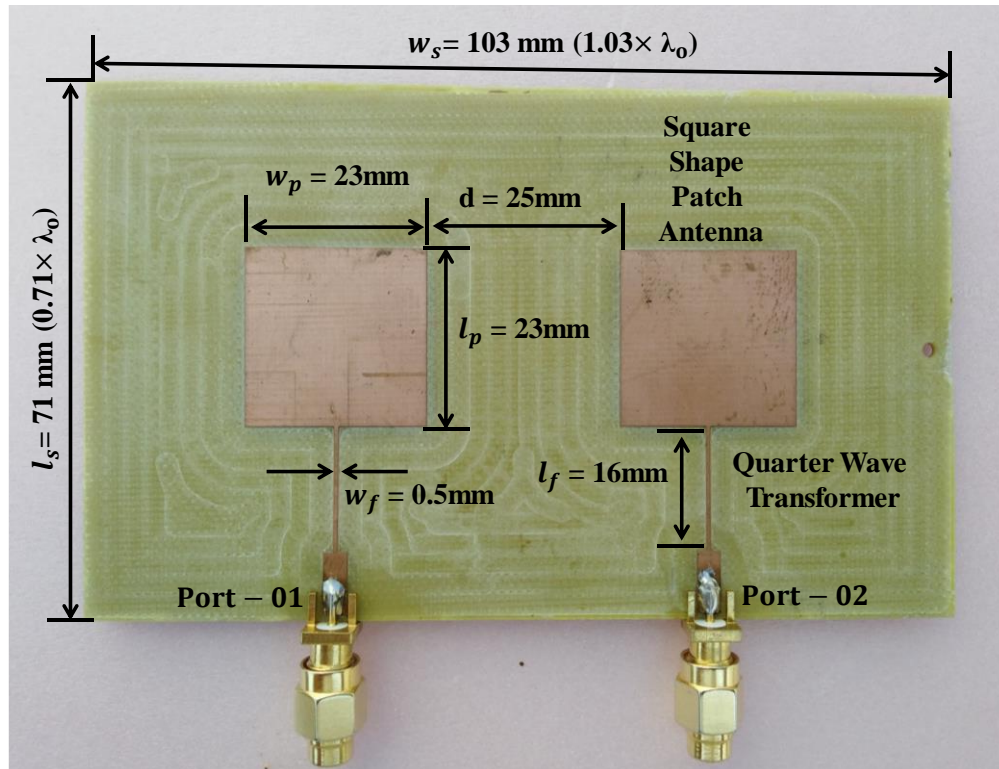

Figure 1.1: Fabricated prototype of 1×2 array antenna

Moreover, the quarter wave impedance transformer ($l_f = 16mm, w_f = 0.5mm$) has been employed to match the input impedance of the square shape patch antenna with the characteristic impedance of 50 Ω. The simulated and measured reflection coefficients for the prototype of the array antenna are given in Figure. 1.12. The results indicate that both ports are well matched with

-10 dB impedance bandwidth of 60 MHz ranging from 2.90 to 2.96 GHz. The frequency shifts between the simulated and measured results can be caused by the various factors including variations in the dielectric constant of substrate, fabrication errors etc.
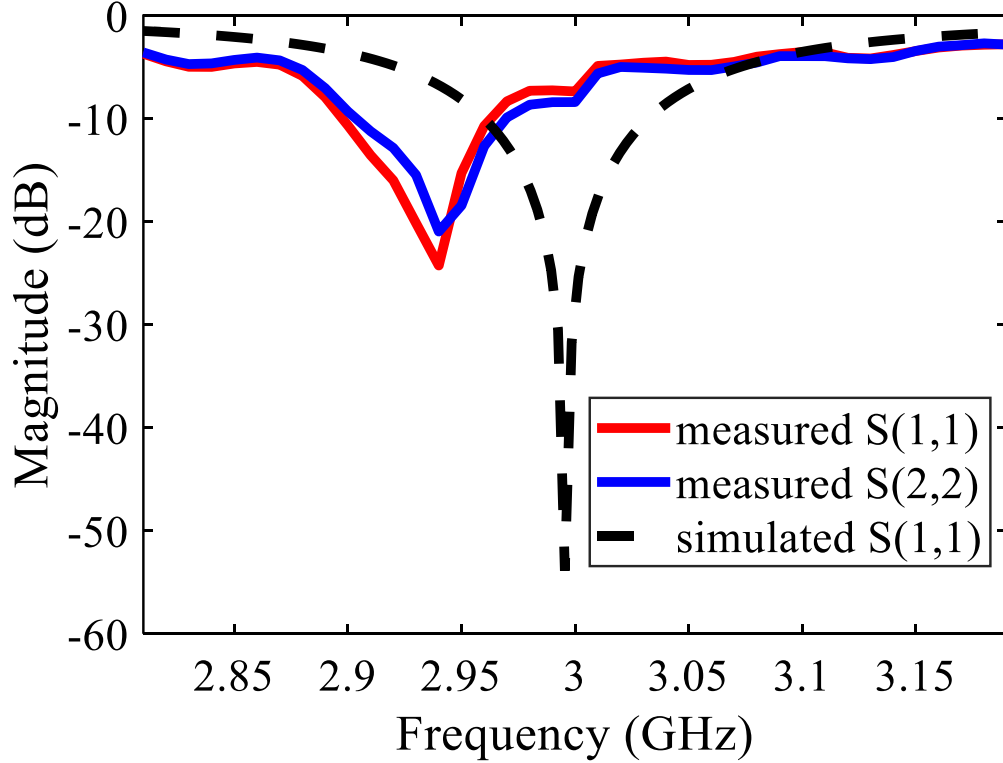

Figure 1.2: Measured reflection coefficients for the prototype of 1×2 array antenna.

Next, the photograph of implemented 180° hybrid coupler is shown in Figure. 1.13. The scattering matrix of 3 dB / 180° hybrid coupler is written as,

$$[S] = \left(\frac{-j}{\sqrt{2}}\right) \times \begin{bmatrix} 0 & 1 & 1 & 0 \\ 1 & 0 & 0 & -1 \\ 1 & 0 & 0 & 1 \\ 0 & -1 & 1 & 0 \end{bmatrix}$$

The -3 dB equal power with phase difference of 0° and 180° is realized between port-2 and port-3, when port-1 and port-4 are excited respectively. The measured reflection coefficient $|S_{ij}|$ i=j=1,2,3,4 are plotted in Figure. 1.14. The results show that all four ports are well matched for frequency ranging from 2.90 to 2.96 GHz. Next the magnitude and phase response of forward transmission coefficient |Sij| ; (i≠j) of 180° ring hybrid coupler between input port-1 and output

ports i.e., 2,3 are given in Figure. 1.15 and Figure. 1.16. The insertion loss is recorded to be around (3.5 ± 0.2) dB whereas phase response is noted to be 0° between input port-1 and output ports i.e., 2,3 for frequency ranging from 2.90 to 2.96 GHz.
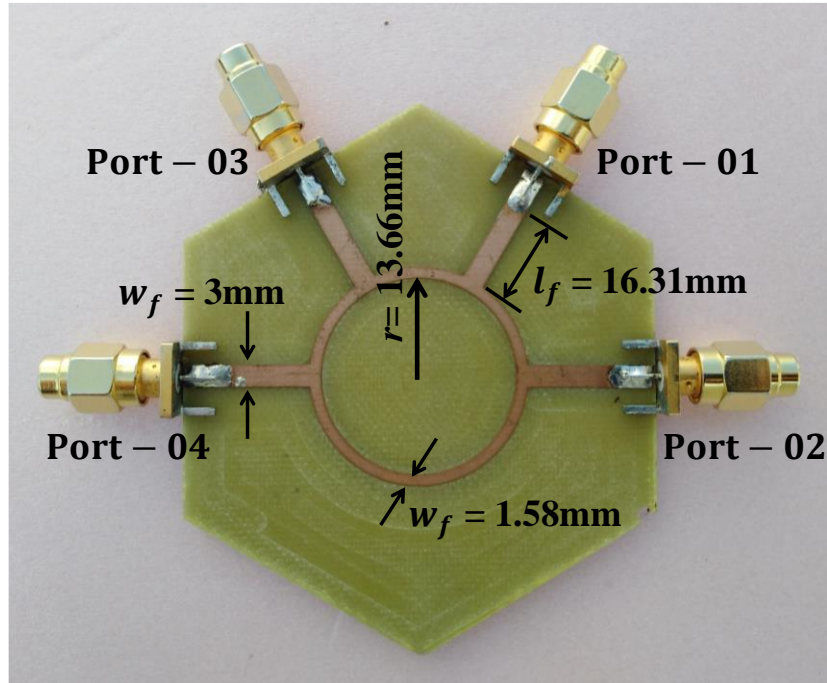

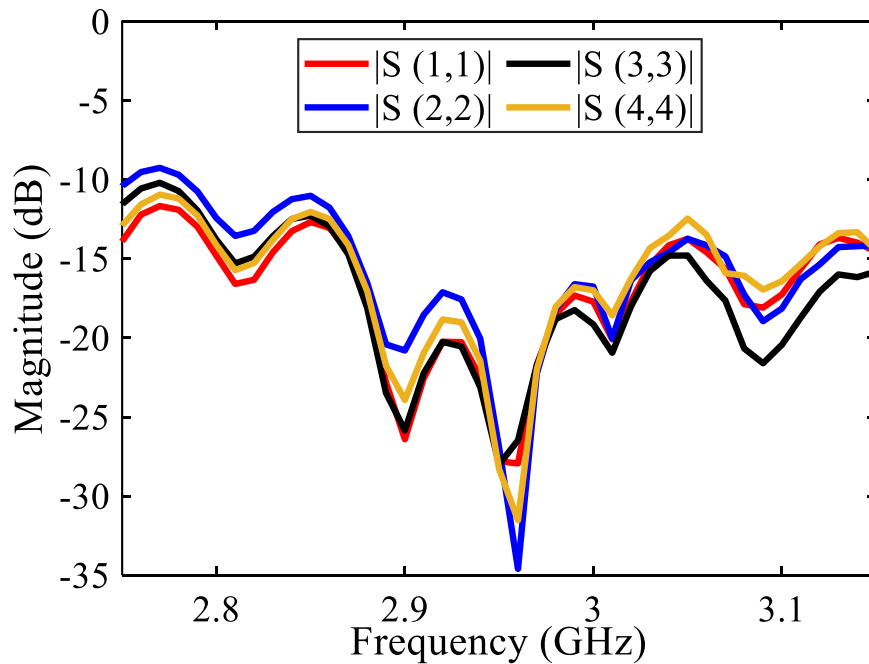**Figure 1.3:** Fabricated prototype of 180° ring hybrid coupler.

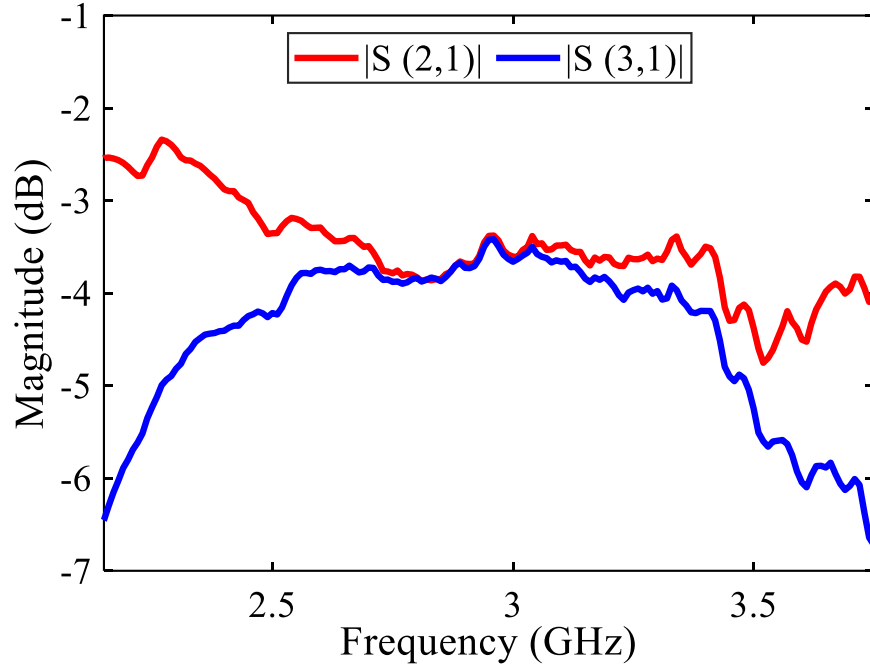**Figure 1.4:** Measured return losses of 180° ring hybrid coupler.

Figure 1.5: Measured magnitude of forward transmission coefficient $|S_{ij}|$; (i≠j) of 180° ring hybrid coupler between input port-1 and output ports i.e., 2,3.
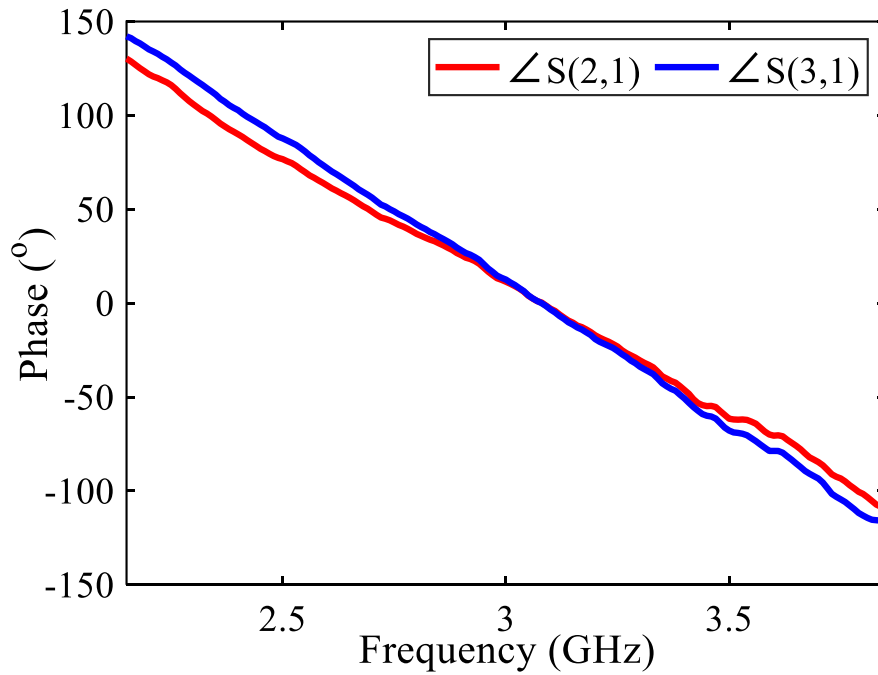

Figure 1.6: Measured phase response of forward transmission coefficient $|S_{ij}|$; (i≠j) of 180° ring hybrid coupler between input port-1 and output ports i.e., 2,3.

Likewise, the magnitude and phase response of forward transmission coefficient |Sij| ; (i≠j) of 180º ring hybrid coupler between input port-4 and output ports i.e., 2,3 are given in Figure. 1.17 and Figure. 1.18. The insertion loss is recorded to be around (3.4 ± 0.2) dB whereas phase response is noted to be 178º between input port-1 and output ports i.e., 2,3 for frequency ranging from 2.90 to 2.96 GHz.
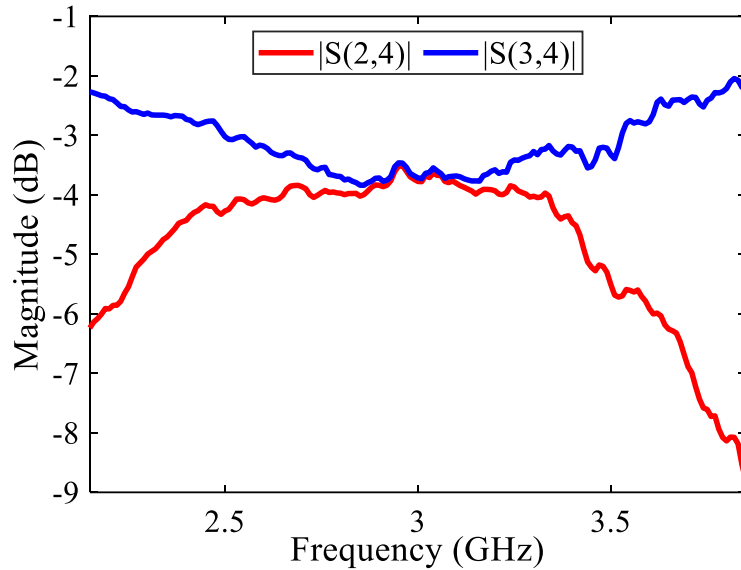
Figure 1.7: Measured magnitude of forward transmission coefficient |Sij| ; (i≠j) of 180º ring hybrid coupler between input port-4 and output ports i.e., 2,3.

Figure 1.8: Measured phase response of forward transmission coefficient |Sij| ; (i≠j) of 180º ring hybrid coupler between input port-4 and output ports i.e., 2,3.

Next, the photograph of implemented 90° hybrid coupler is shown in Figure. 1.19. The measured reflection coefficient $|S_{ij}|$ i=j=1,2,3,4 are plotted in Figure. 1.20. The results show that all four ports are well matched for frequency ranging from 2.90 to 2.96 GHz. Next the magnitude and phase response of forward transmission coefficient |Sij| ; (i≠j) of 180° ring hybrid coupler between input port-1 and output ports i.e., 2,3 are given in Figure. 1.21 and Figure. 1.22. The insertion loss is recorded to be around (3.8 ± 0.8) dB whereas phase response is noted to be 87° between input port-1 and output ports i.e., 2,3 for frequency ranging from 2.90 to 2.96 GHz.


Figure 1.9: Fabricated prototype of 90° ring hybrid coupler.

Figure 1.10: Measured return losses of 90° ring hybrid coupler.

Figure 1.11: Measured magnitude of forward transmission coefficient $|S_{ij}|$; $(i \neq j)$ of 90° hybrid coupler between input port-1 and output ports i.e., 2,3.
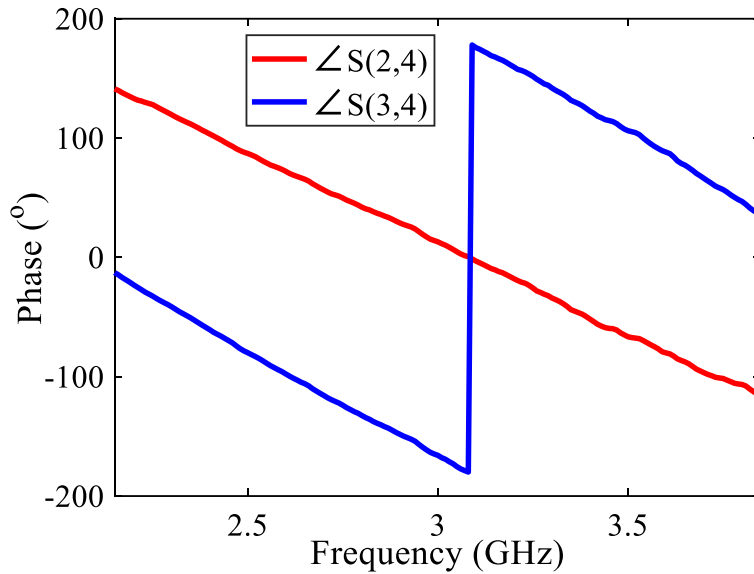

Figure 1.12: Measured phase response of forward transmission coefficient $|S_{ij}|$; $(i \neq j)$ of 90° hybrid coupler between input port-1 and output ports i.e., 2,3.

Likewise, the magnitude and phase response of forward transmission coefficient |Sij| ; (i≠j) of 90º ring hybrid coupler between input port-4 and output ports i.e., 2,3 are given in Figure. 1.23 and Figure. 1.24. The insertion loss is recorded to be around (4 ± 0.8) dB whereas phase response is noted to be −89° between input port-1 and output ports i.e., 2,3 for frequency ranging from 2.90 to 2.96 GHz.
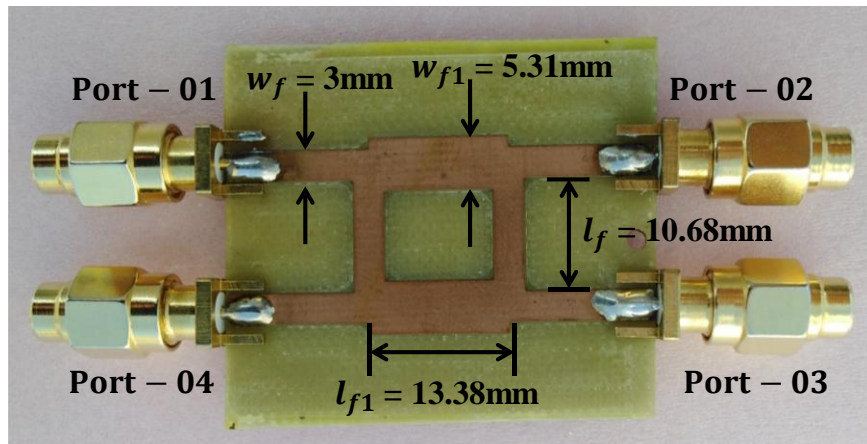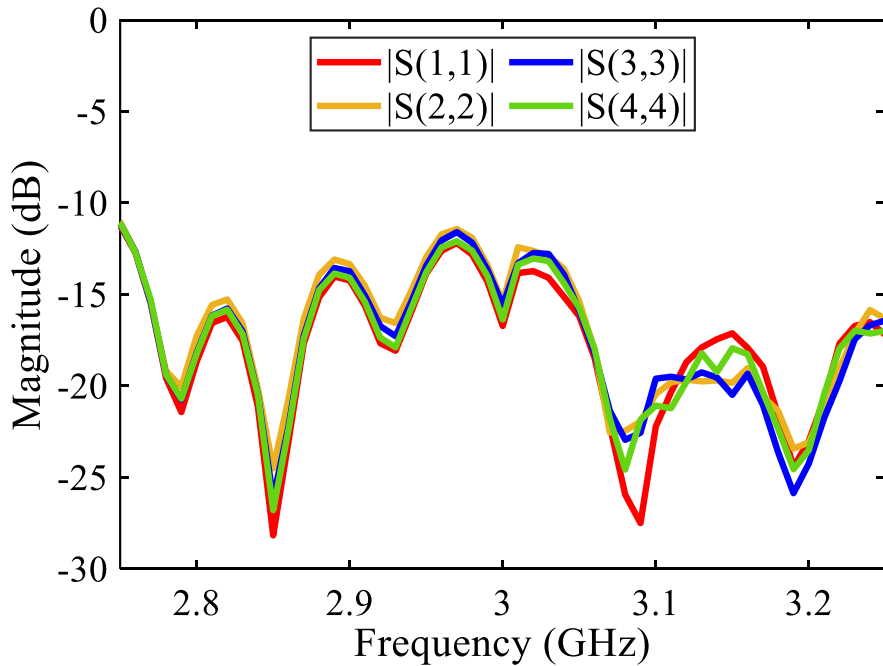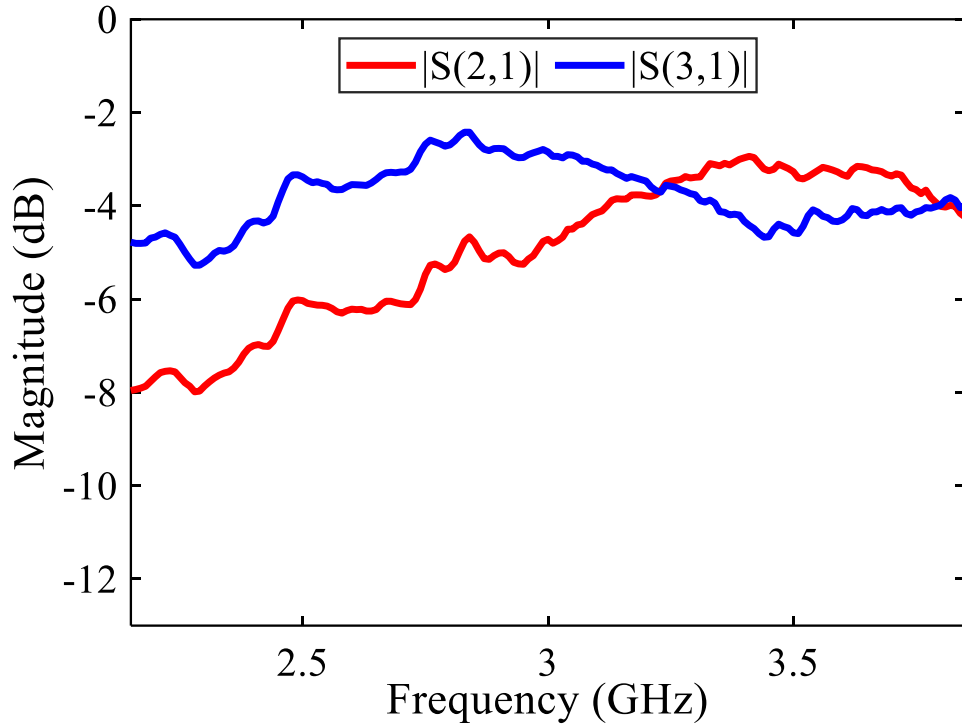

Figure 1.13: Measured magnitude response of forward transmission coefficient |S$_{ij}$| ; (i≠j) of 90º hybrid coupler between input port-4 and output ports i.e., 2,3.
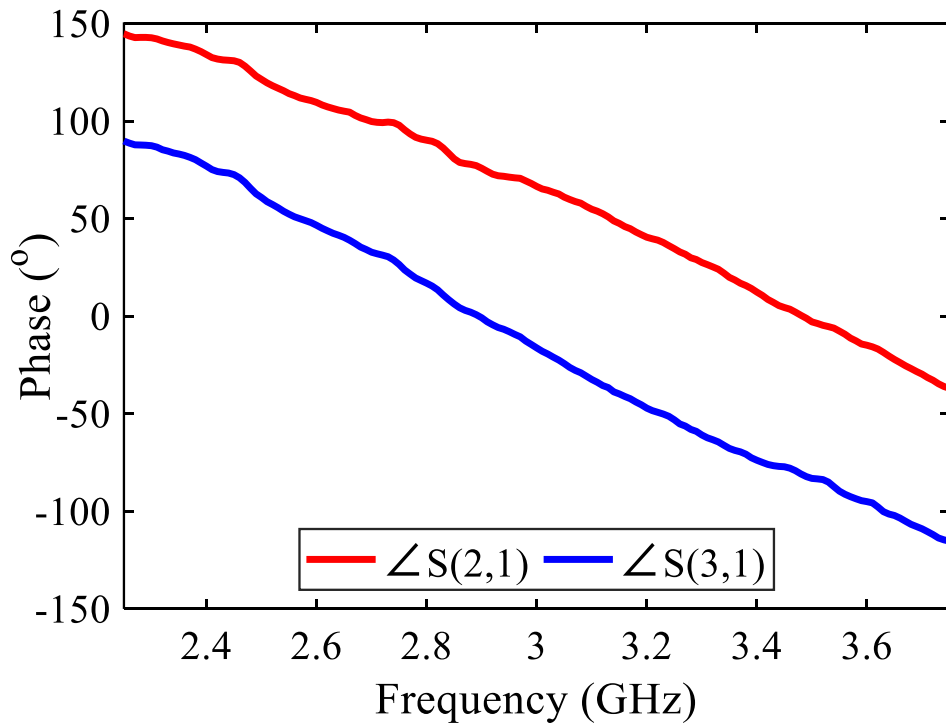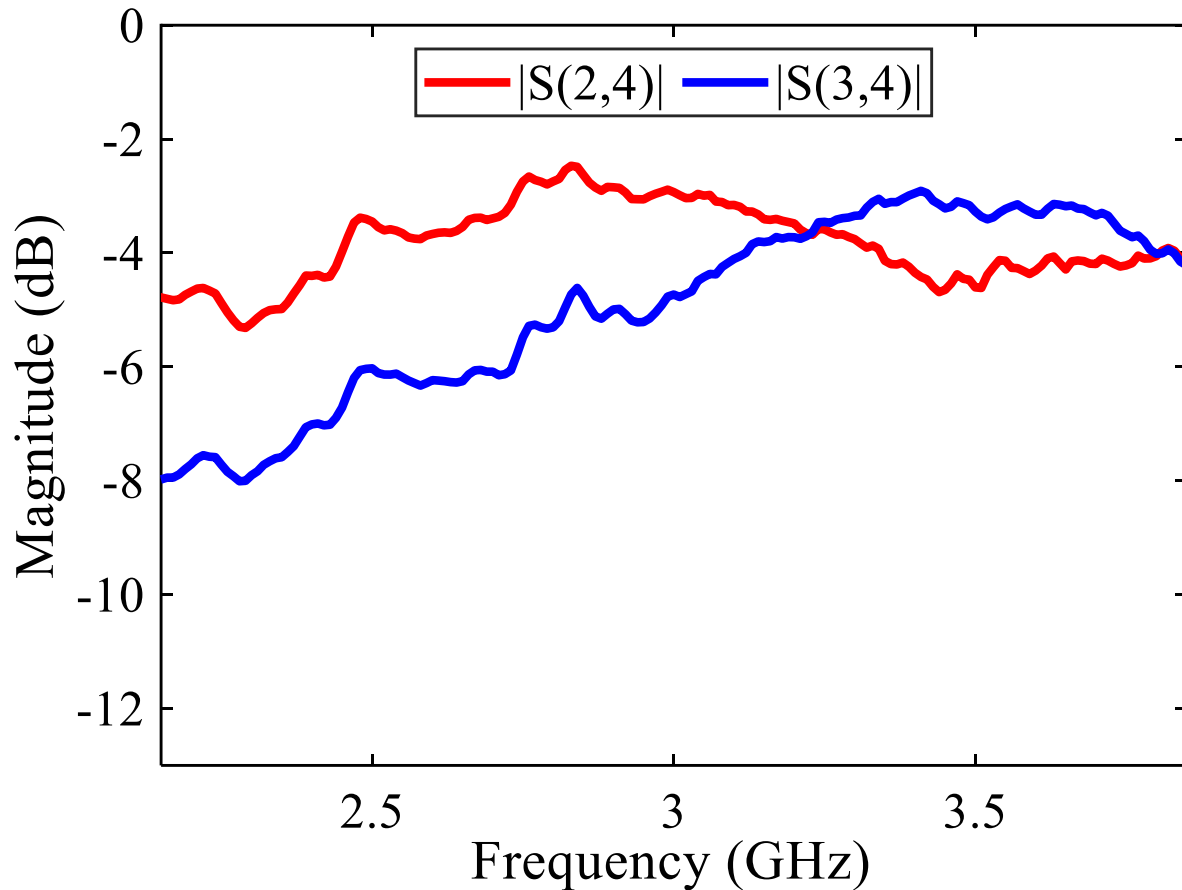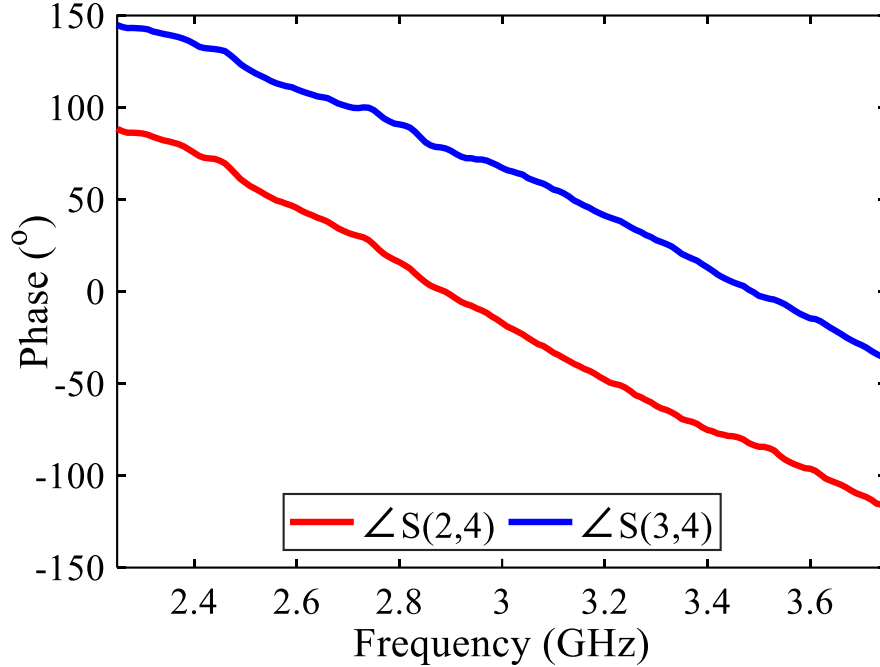
Figure 1.14: Measured phase response of forward transmission coefficient $|S_{ij}|$; (i≠j) of 90° hybrid coupler between input port-4 and output ports i.e., 2,3.

Next the RF absorptive switches i.e., Single-Pole-Double-Throw (SP2T) and Single-Pole-Quadruple-Throw (SP4T) have been incorporated in the circuit. The SP2T switches are utilized to interconnect the intended hybrid couplers with the antenna ports independently. The SP4T switch is incorporated in the circuit to interconnect the output ports of the hybrid couplers with a single envelope detector for a cost effective solution. The evaluation board of Absorptive SPDT Switch i.e., Renesas-F2932 is shown in Figure. 1.25. The magnitude responses i.e., isolation and insertion loss; phase responses are mentioned in Figure 1.26. Likewise, the truth table of control signals i.e., control voltages (VCTL) is given in Table 1-2.

Table 1-1: Switch Control Truth Table

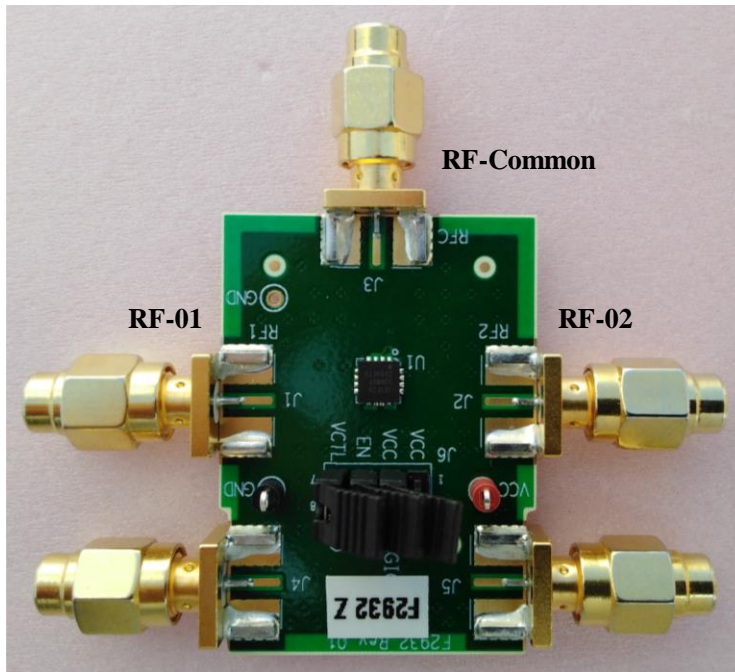| VCTL	EN	RFC to RF1	RFC to RF2
0	1	OFF	OFF
1	1	OFF	OFF
0	0	OFF	ON
1	0	ON	OFF

Figure 1.15: Evaluation Board of Absorptive SPDT Switch i.e., Renesas-F2932
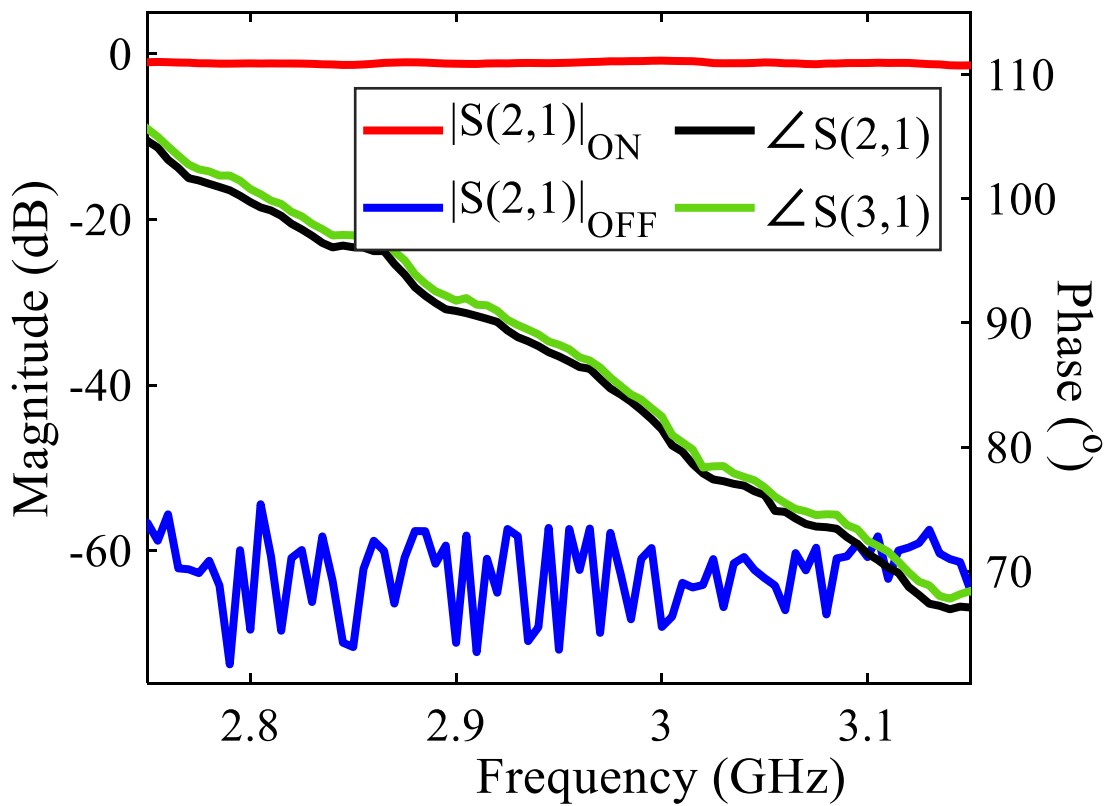

Figure 1.16: Measured S-parameters of Absorptive SPDT Switch i.e., Renesas-F2932)

At f_0 = 2.94 GHz, the simulated and measured monopulse function ($\frac{\Delta}{\Sigma}$) is in well agreement for a FoV [-30⁰ +30⁰] as shown in Figure. 1.28.

For the given length, the maximum insertion loss of coaxial cables is recorded to be 0.643 dB whereas the hybrid coupler provides the 3 dB coupling from the input to output ports at f_0 = 2.94 GHz. To validate the system performance, the measured DoA estimations along with angle estimation error i.e., root-mean-square-error (RMSE) are also presented in Figure. 1.28. The measured AoA has been determined using (3) with measured monopulse function ($\frac{\Delta}{\Sigma}$). The results show that, maximum RMSE is recorded to be less than 5⁰ for given FoV of 60⁰ ranges from -30⁰ to +30⁰ except at -20⁰ where RMSE is noted to be 8.9⁰. It can also be observed that due to monotonic behavior of monopulse function, the measured AoA is same for both negative and positive angle-of-arrivals. This angular ambiguity would be resolved while comparing the amplitude of received signal from the additional switched beams as described in Section 1.2.1.

To characterize the 2-D radiation patterns in an anechoic chamber, a standard horn antenna used as a transmitting antenna is kept at 3.40 m from the antenna under test (AUT). The power is received by the AUT with a scanning rate of 4.4 deg./sec. The radiation patterns of the presented array antenna have been characterized in the 360⁰ span (θ = 180⁰ to θ = -180⁰) for both φ = 0⁰ and φ = 90⁰ in anechoic chamber.

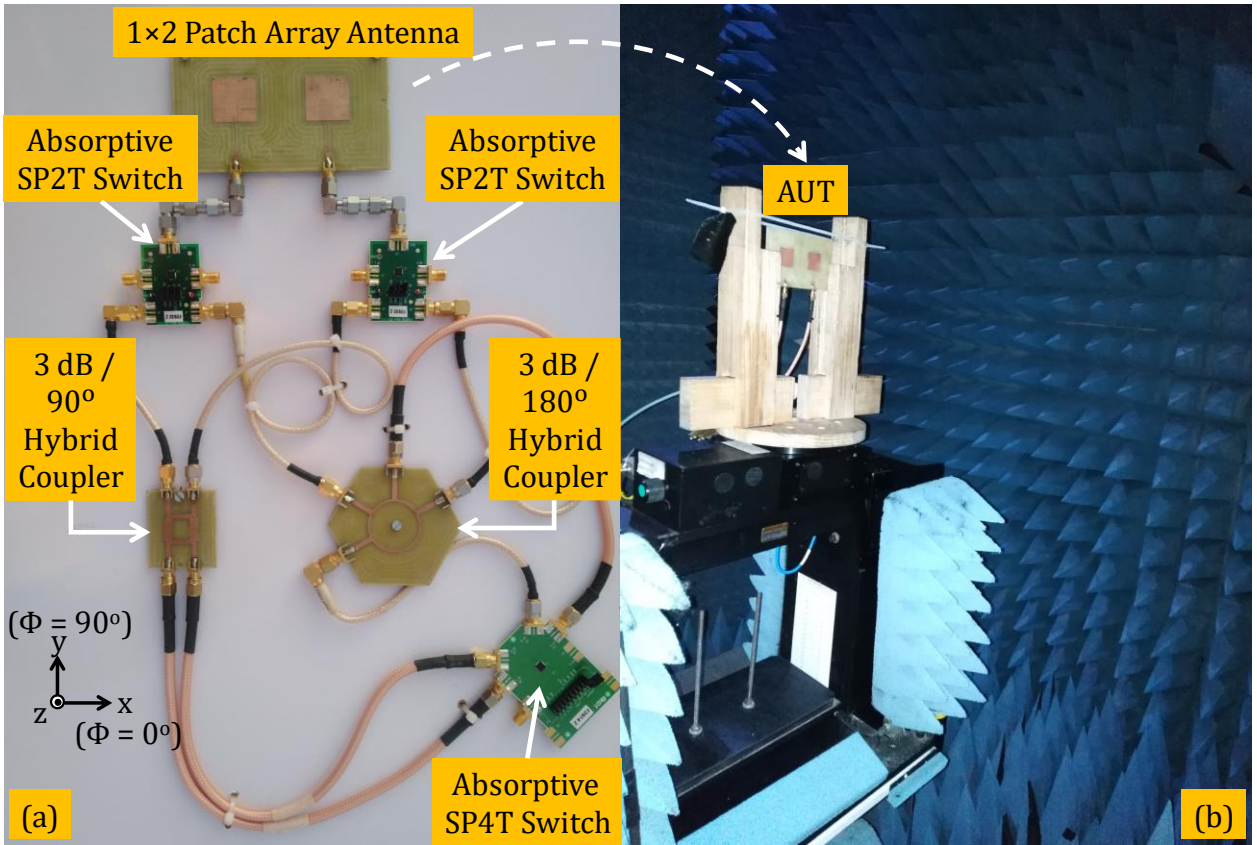**Figure 1.17:** Left Side: Photograph of proposed DF antenna system ; Right Side: Measured reflection coefficients for the prototype of 1×2 array antenna.

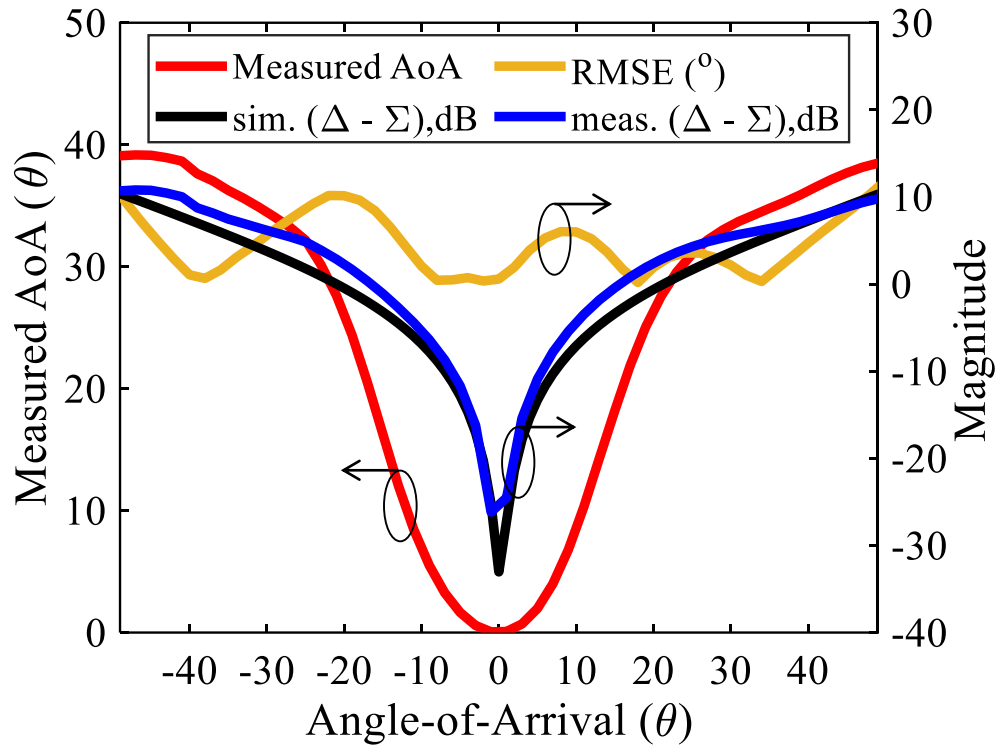**Figure 1.18:** Simulated and measured relationship between the monopulse function (Δ/Σ) and AoA (θ) at 2.94 GHz.
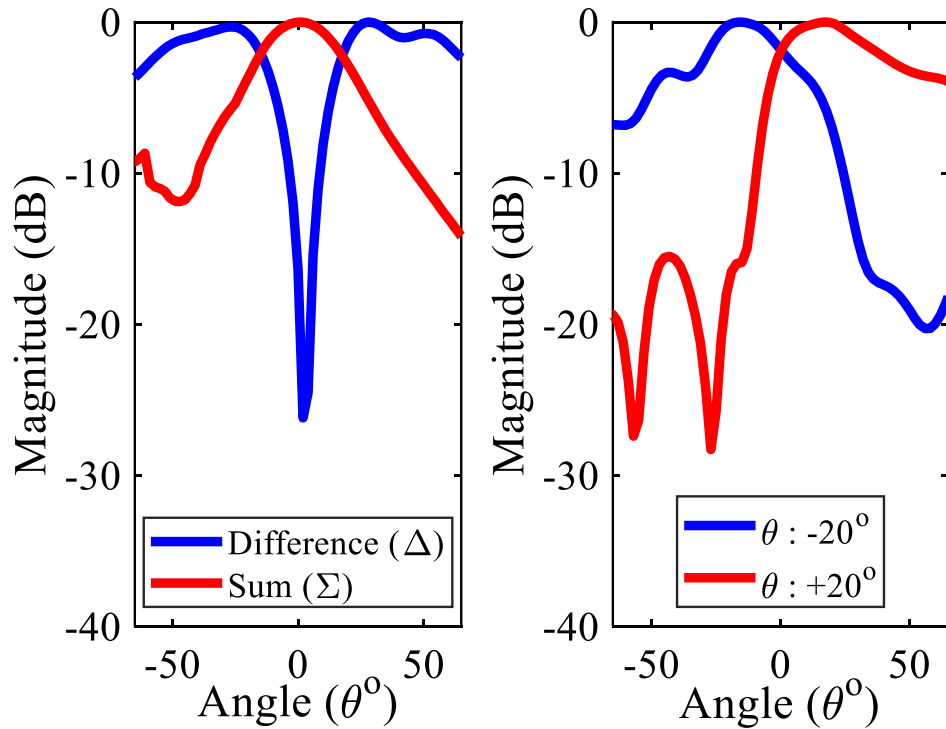

Figure 1.19: Measured normalized gain plots of the four switched beams at 2.94 GHz in the xoz-plane.

Due to antenna's geometry, the main beam will be switched in xoz-plane. For the sake of brevity, the measured normalized gain plots at 2.94 GHz in the xoz-plane are plotted in Figure. 1.29. The maximum measured peak gain for the sum-pattern and difference pattern is recorded to be respectively 5.97 dBi and 3.97 dBi with radiation efficiency of 55%. Likewise, the magnitude of two switched beams and null depth of difference pattern is recorded to be 5.1 dBi and -25 dB respectively. The gain difference between simulated and measured patterns is because of surface roughness of copper, loss tangent (tanδ) of substrate and fabrication errors. Consequently, the proposed antenna system can be employed to compute the DoA while resolving the angular ambiguity in the FoV using additional switched beams. In order to highlight the contributions and novelty of this work, the performance comparison of the presented antenna system with the recent reported work is summarized in Table 1-4,

Table 1-2: Performance comparison of presented antenna with recent reported amplitude monopulse antenna systems

References.	Centre Frequency	Bandwidth	Field-of-View	Angular Ambiguity Resolution Schemes	Remarks
[3]	9.85 GHz	149 MHz	76º	RF-Multiplier	o At higher frequencies, the cost of such phase comparator is increased o Planar Antenna. o Active and Passive DF.
[4]	866.5 MHz	3.0 MHz	50º	Mechanically Rotated Two Antennas	o Non-planar geometry o It can only be used in passive direction finding (DF) systems
[5]	2.45 GHz	Not Given.	50º		
[6]	2.45 GHz	20 MHz	60º		
This Work	2.93 GHz	60 MHz	60º	Orthogonal Switched Beams	o It can be used for frequency > 3GHz. o Monopulse DF + Sequential Lobing DF o Planar geometry o It can be employed in both active and passive monopulse DF systems

5. Conclusion

In this chapter, a planar antenna system is presented for amplitude comparison based DF. To validate the concept, the antenna system has been designed for 3 GHz, however this concept is valid for higher frequencies i.e., > 3 GHz. The DF estimation is realized through the mono-pulse and the sequential-lobing techniques. In amplitude monopulse antenna systems, to address the angular ambiguity in the sign (+or-) associated with AoA, phase-based power summation property of 90° hybrid coupler and the corresponding switched-beams have been utilized.

5.1 Future Work

In future work, this work can be extended for wideband DF applications, in that case, wideband radiating structure, 3dB/90° Hybrid coupler, 3dB/180° Hybrid coupler, RF switches would be required.

6. Acknowledgement

7. References

[1]   Sherman. S.M., Burton. D.K, "Monopulse Principles and Techniques", 2nd ed, Artech House, Norwood, MA, USA, 2011.

[2]   J. Xie, X. Feng, Y. Yuan, and S. Li, "Application of monopulse techniques in angle-measuring of single-beam mechanical scanning radar," Proc. 3rd Int. Congr. Image Signal Process., pp. 2971–2974, 2010.

[3]   Rashid, Rimi et al. "A Planar Extended Monopulse DoA Estimation Antenna Integrating an RF Multiplier." Progress in Electromagnetics Research C 81, pp. 53-62, 2018.

[4]   Y. Álvarez-López, M. E. Cos-Gómez, and F. Las-Heras-Andrés, "A received signal strength RFID-based indoor location system,", Sensors and Actuators A: Physical, vol. 255, pp. 118–133, 2017, doi.org/10.1016/j.sna.2017.01.007

[5]   M. Poveda-García et al., "Amplitude-Monopulse Radar Lab Using WiFi Cards," 2018 48th European Microwave Conference (EuMC), Madrid, Spain, 2018, pp. 464-467, doi: 10.23919/EuMC.2018.8541674.

[6]   J. A. López-Pastor, P. Arques-Lara, J. J. Franco-Peñaranda, A. J. García-Sánchez and J. L. Gómez-Tornero, "Wi-Fi RTT-Based Active Monopulse RADAR for Single Access Point Localization," IEEE Access, vol. 9, pp. 34755-34766, 2021.

[7]   C.A. Balanis,"Antenna Theory Analysis and Design," 4th edition, Wiley& Sons, New York, 2016.

[8]   W.L. Stutzman and G.A. Thiele, "Antenna Theory and Design,"3rd ed, Wiley & Sons, New York, 2012.

[9]   N. Shoaib, "Vector Network Analyzer (VNA) Measurements and Uncertainty Assessment," Springer, vol. 1; pp. 1-82, 2017. Available Online at: https://doi.org/10.1007/978-3-319-44772-8

8. Appendices

8.1 Appendix-A

    Based on array factor theory, two isotropic point sources which are spatially displaced $\frac{3\lambda}{4}$ apart when excited with identical amplitude and phase difference of 0° / 180°, a sum and difference pattern is synthesized respectively.

For sum pattern:

$$AF = 1 \times e^{-j\beta\left(\frac{d}{2}\right)\sin\theta} + 1 \times e^{j\beta\left(\frac{d}{2}\right)\sin\theta} = 2\cos\left(\frac{\beta d}{2} \times \sin\theta\right)$$

$$f(\theta) = \Sigma = \cos\left(\frac{\beta d}{2} \times \sin\theta\right) \qquad\qquad (1)$$

For difference pattern:

$$AF = -1 \times e^{-j\beta\left(\frac{d}{2}\right)\sin\theta} + 1 \times e^{j\beta\left(\frac{d}{2}\right)\sin\theta} = 2j\sin\left(\frac{\beta d}{2} \times \sin\theta\right)$$

$$f(\theta) = \Delta = \sin\left(\beta\frac{d}{2} \times \sin\theta\right) \qquad\qquad (2)$$

Dividing (2) and (1)

$$\frac{\Delta}{\Sigma} = \frac{\sin\left(\beta\frac{d}{2} \times \sin\theta\right)}{\cos\left(\beta\frac{d}{2} \times \sin\theta\right)}$$

$$\frac{\Delta}{\Sigma} = \tan\left(\beta\frac{d}{2} \times \sin\theta\right)$$

$$\tan^{-1}\left(\frac{\Delta}{\Sigma}\right) = \left(\beta\frac{d}{2} \times \sin\theta\right)$$

$$\sin\theta = \left(\frac{2}{\beta d} \times \tan^{-1}\left(\frac{\Delta}{\Sigma}\right)\right)$$

$$\sin\theta = \left(\frac{2}{\beta d} \times \tan^{-1}\left(\frac{\Delta}{\Sigma}\right)\right)$$

$$\theta = \sin^{-1}\left(\frac{2}{\beta d} \times \tan^{-1}\left(\frac{\Delta}{\Sigma}\right)\right)$$

Putting $\beta = \frac{2\pi}{\lambda}$

$$\theta = \sin^{-1}\left(\frac{2}{\frac{2\pi}{\lambda}d} \times \tan^{-1}\left(\frac{\Delta}{\Sigma}\right)\right)$$

$$\boldsymbol{\theta = sin^{-1}\left(\frac{\lambda}{\pi d} \times tan^{-1}\left(\frac{\Delta}{\Sigma}\right)\right)}$$